Supporting information

Effect of oxygen vacancies on the plasma-catalytic performance of CeO_2 for CO_2 hydrogenation

Joran Van Turnhout[1,2,3,4], Wouter Van Hoey[5], Shangkun Li[1, 2, 4, 6], Robin De Meyer[1, 2, 4, 7], Morgane Van Hove[1, 5], Thomas Salens[2, 7], Johan Verbeeck[2, 7], Sara Bals[7], Bart Partoens[2, 6], Emiel Hensen[3*], Pegie Cool[5] and Annemie Bogaerts[1,2,4*]

[1]Research group PLASMANT, Department of Chemistry, University of Antwerp, Groenenborgerlaan 171, 2020 Antwerp, Belgium

[2]Center of Excellence PLASMA, University of Antwerp, Groenenborgerlaan 171, 2020 Antwerp, Belgium

[3]Laboratory of Inorganic Materials and Catalysis, Department of Chemical Engineering and Chemistry, Eindhoven University of Technology, P.O. Box 513, 5600 MB Eindhoven, Netherlands

[4]Electrification Institute, University of Antwerp, Olieweg 97, 2020 Antwerp, Belgium

[5]Research group LADCA, Department of Chemistry, University of Antwerp, Groenenborgerlaan 171, 2020 Antwerp, Belgium

[6]Research group COMMIT, Department of Physics, University of Antwerp, Groenenborgerlaan 171, 2020 Antwerp, Belgium

[7]Research group EMAT, Department of Physics, University of Antwerp, Groenenborgerlaan 171, 2020 Antwerp, Belgium

[*]Corresponding authors

Table of Contents

S1. Experimental methods

Table S1: Average plasma power during the experiments for all samples.

	Average plasma power (W)
Plasma only	26 ± 3
CeO_2	26 ± 1
CeO_2-Ar	26 ± 1
CeO_2-PR	26 ± 1
CeO_2-TR	27 ± 1
3 wt% Cu/CeO_2	27 ± 2

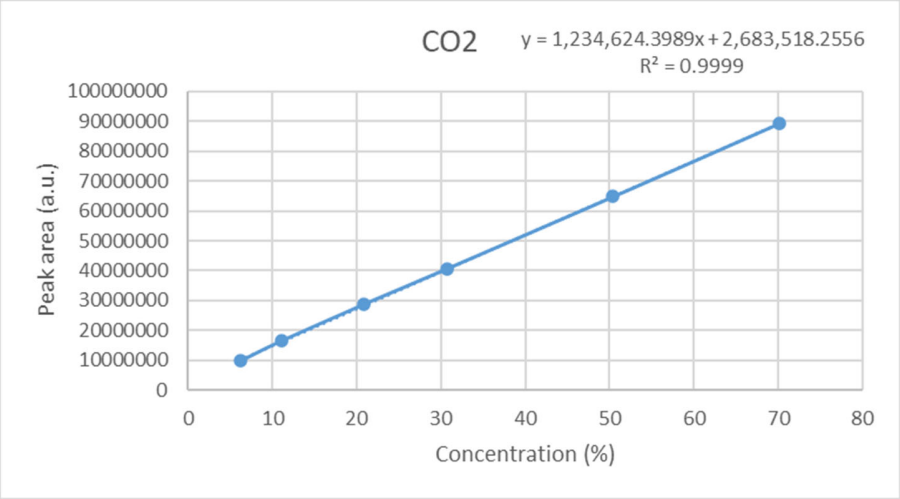

Figure S1: GC calibration curve for CO_2

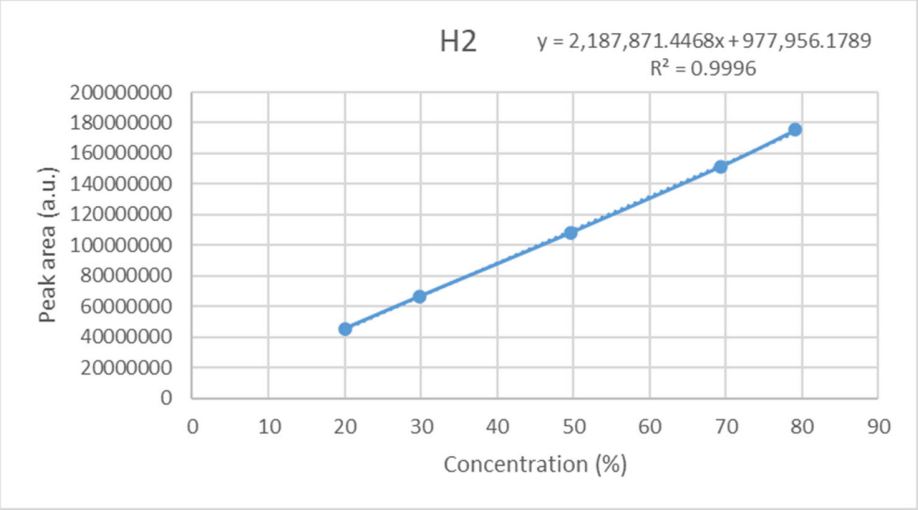

Figure S2: GC calibration curve for H_2

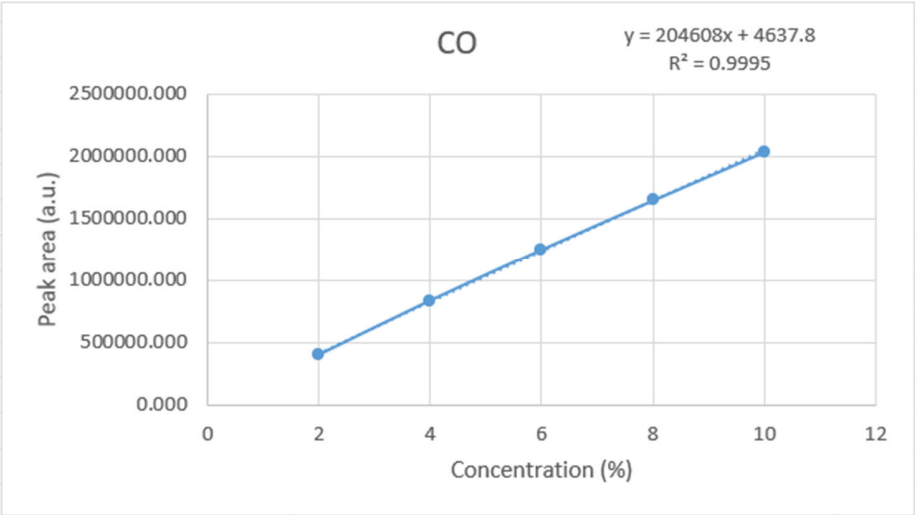

Figure S3: GC calibration curve for CO

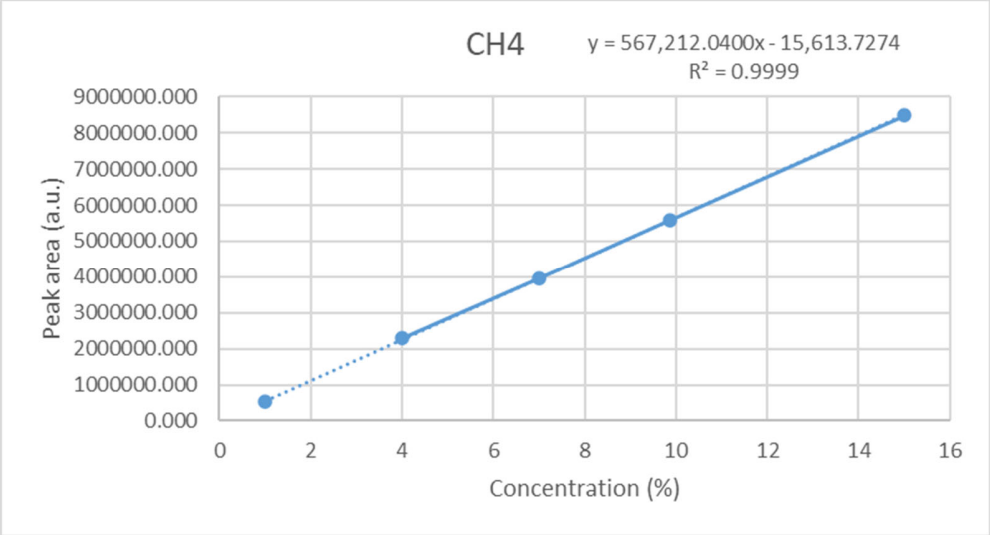

Figure S4: GC calibration curve for CH_4

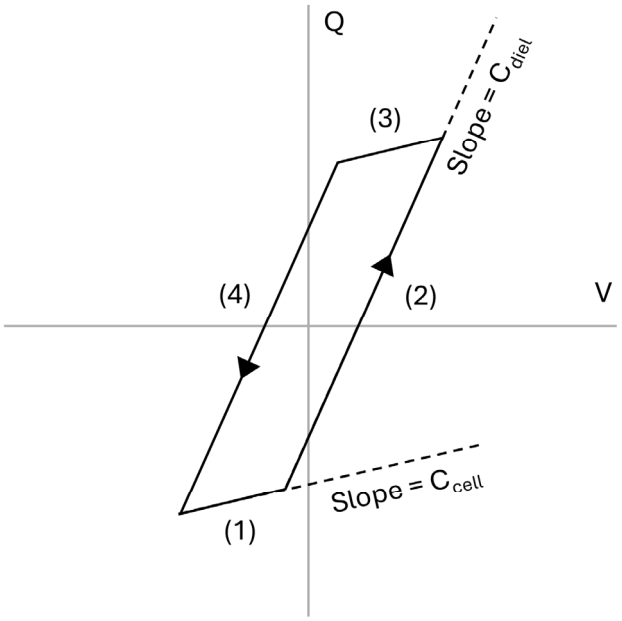

Figure S5: Illustration of the ideal Q-V diagram (called Lissajous figure) with parameters that can be extracted. Slopes (1) and (3) represent the "plasma off" phase, while slopes (2) and (4) represent the "plasma on" phase. More information can be obtained from Peeters and van de Sanden[1].

S2. Catalyst characterization

S2.1 N_2-sorption

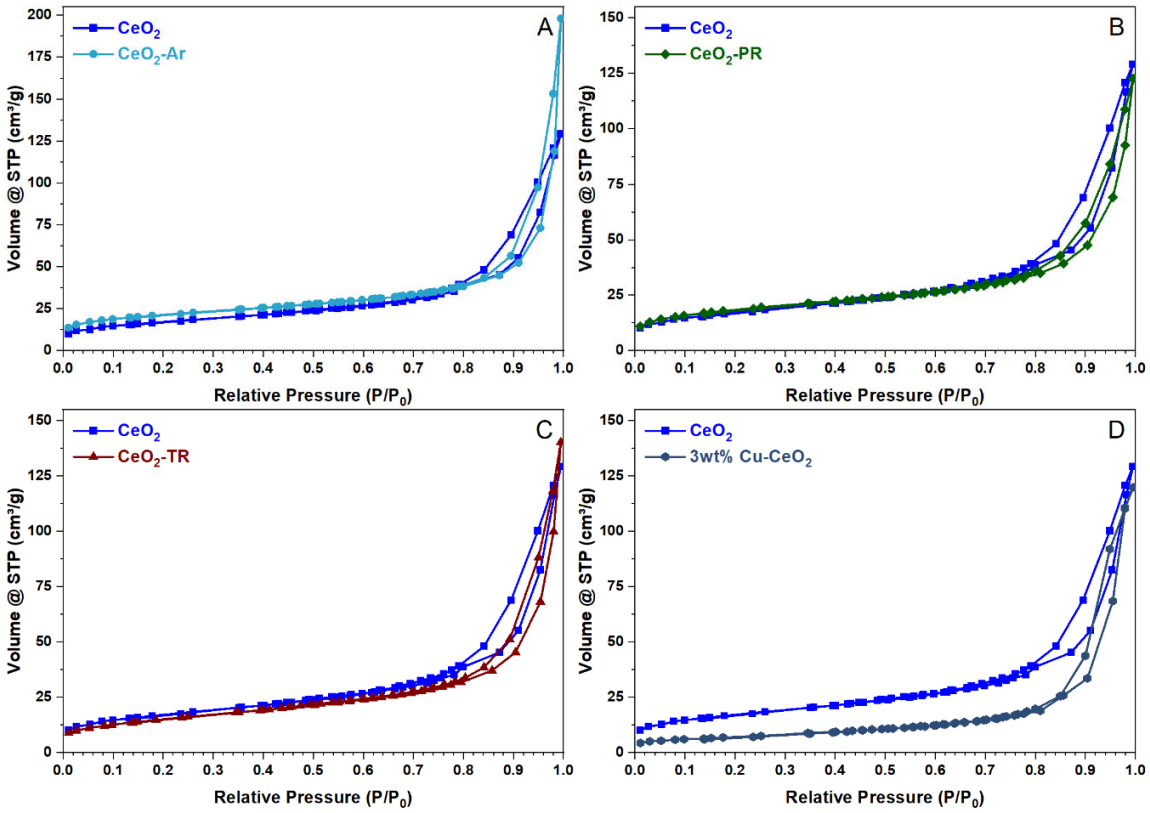

Figure S6: N_2-sorption isotherms of CeO_2 (A), CeO_2-Ar (B), CeO_2-PR (C), CeO_2-TR (D) and 3wt% Cu-CeO_2

S2.2 XRD

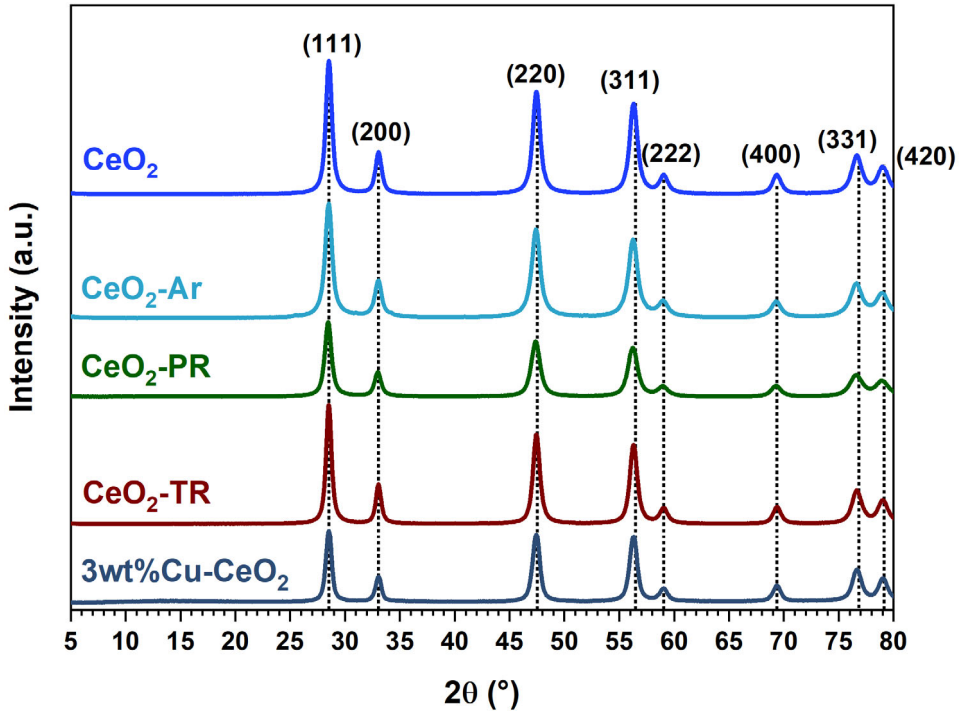

Figure S7: XRD patterns of CeO_2, CeO_2-Ar, CeO_2-PR, CeO_2-TR and 3wt% Cu-CeO_2

S2.3 SEM and TEM

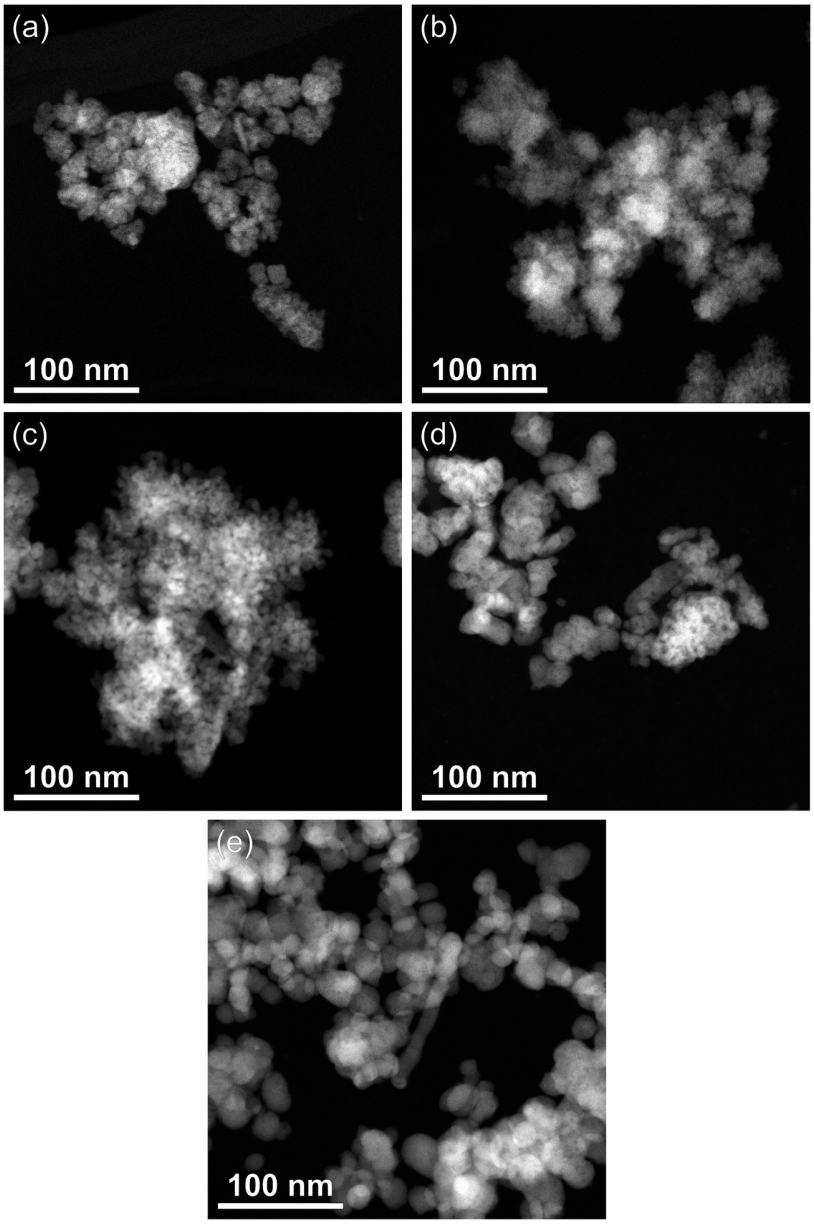

Figure S8: TEM images of (a) CeO_2, (b) CeO_2-Ar, (c) CeO_2-PR, (d) CeO_2-TR, and (e) Cu/CeO_2. Agglomerates of nanoparticles can be observed in all samples.

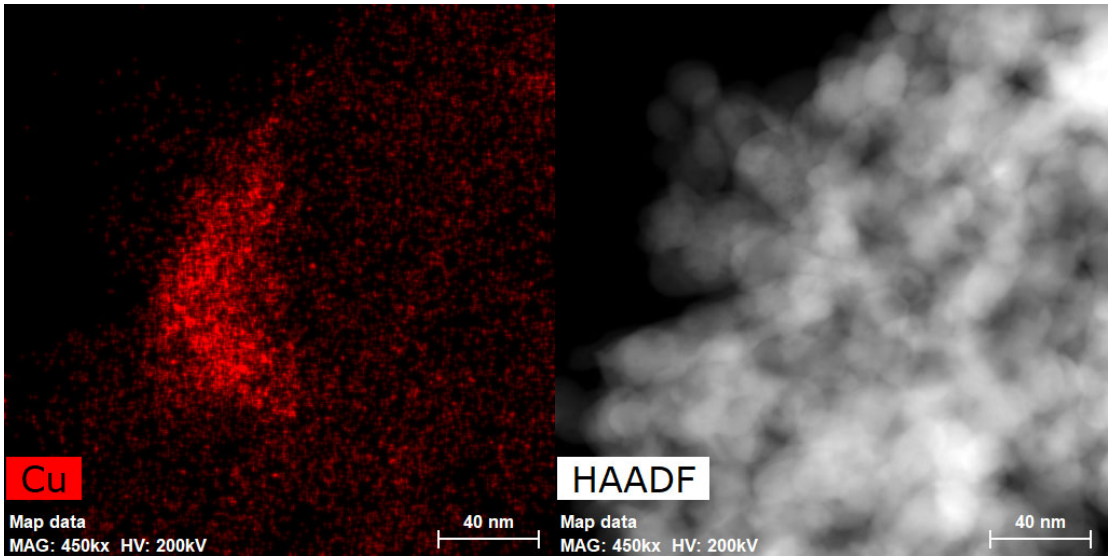

Figure S9: Map of the Cu EDX signal and the corresponding HAADF-STEM image. A clear localized Cu signal is observed, but this does not correspond to a well-defined structure in the HAADF-STEM image, possibly indicating high dispersion of the Cu.

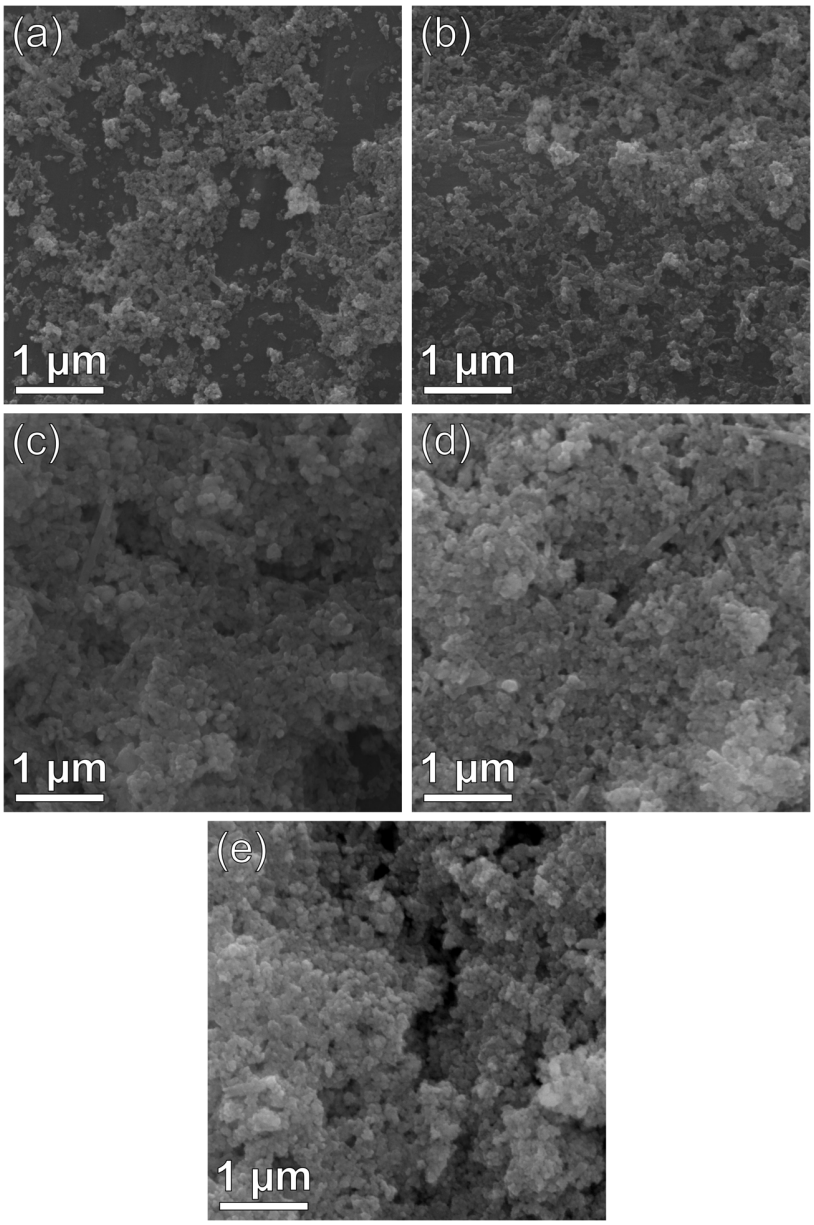

Figure S10: SEM images of (a) CeO_2, (b) CeO_2-Ar, (c) CeO_2-PR, (d) CeO_2-TR, and (e) Cu/CeO_2. In all samples, agglomerations of mostly isotropic particles are observed.

S2.4 Raman

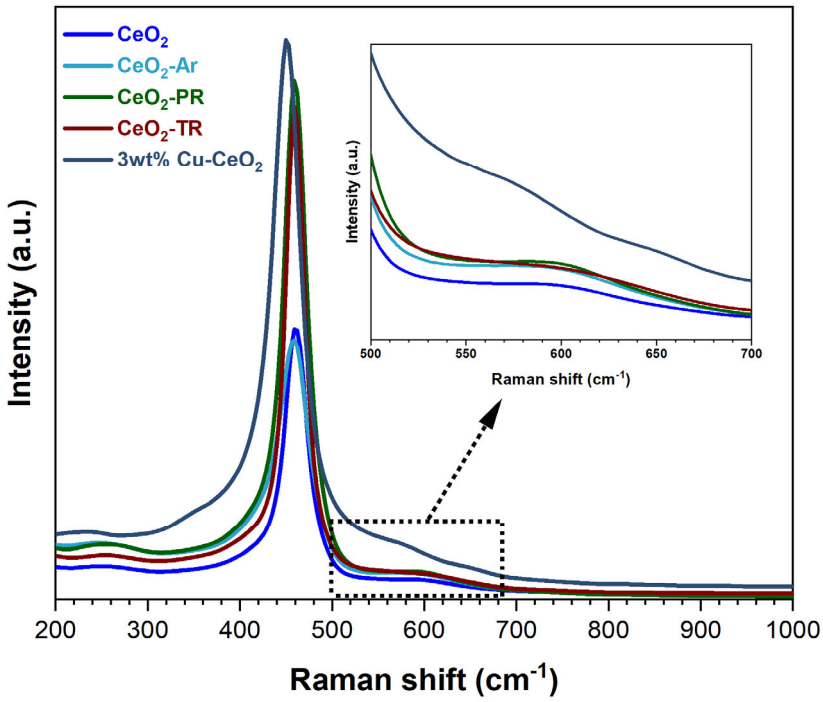

Figure S11: Raman spectra of CeO_2, CeO_2-Ar, CeO_2-PR, CeO_2-TR and 3wt% Cu/CeO_2. The intense band around 460 cm^{-1} is attributed to the F_{2g} Raman mode of CeO_2. The shoulder between 520 and 680 cm^{-1} represents the D-band of CeO_2 and is an indication for the presence of OVs.

S2.5 H_2-TPR

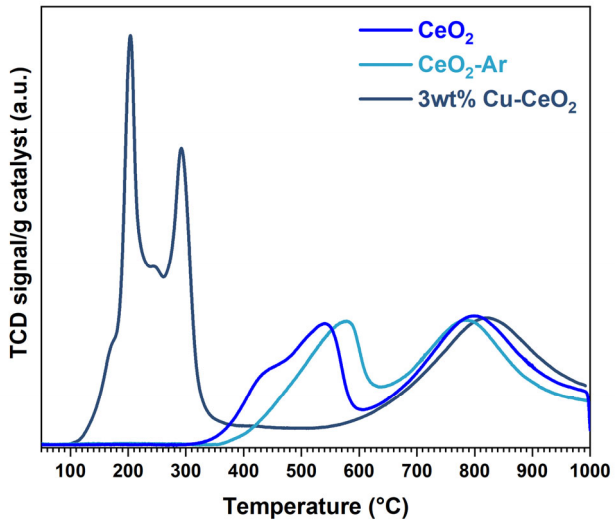

Figure S12: H_2-TPR profiles of CeO_2, CeO_2-Ar and 3wt% Cu/CeO_2. The TPR profile of CeO_2 contains two main reduction features at 530 °C and 780 °C, corresponding to the surface reduction and bulk reduction of Ce^{4+}, respectively. The shoulder before the first main reduction peak indicates the presence of more easily reducible sites at the surface of CeO_2. For 3wt% Cu/CeO_2, the additional reduction signals at 204 °C, 245 °C, and 292 °C represent the reduction of well-dispersed Cu particles, larger CuO particles and a Cu-CeO_2 solid solution, respectively.

S2.6 XPS

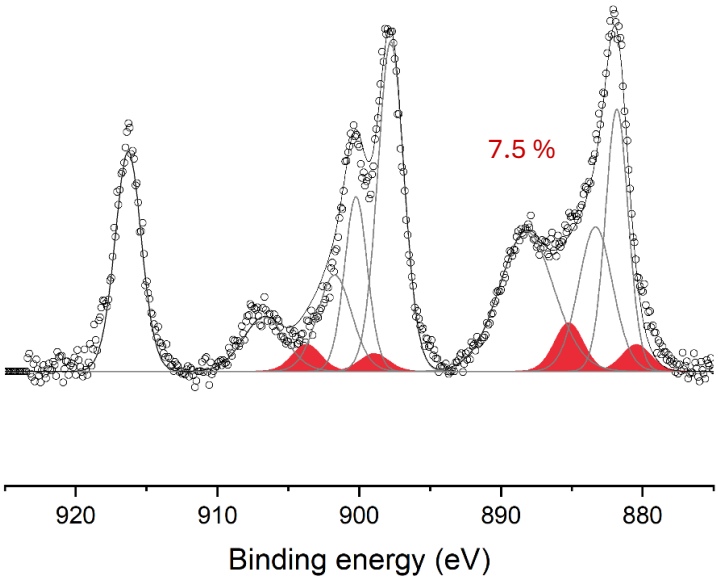

Figure S13: First scan for XPS of Ce 3d for the CeO_2 sample, recorded before survey scan

The Ce^{3+} concentrations given in the main paper are to be interpreted qualitatively, because reduction of Ce^{4+} can be induced during the XPS experiment. To show this effect, we performed an experiment in which the Ce 3d region was scanned first, to limit the reduction of Ce^{4+}. To avoid reduction during consecutive scans, we present the data of the first scan of the Ce 3d region. Figure S10 shows the fitted spectrum of this scan. The Ce^{3+} concentration is determined to be 7.5 %. When the Ce^{3+} concentration is obtained from an average of 50 consecutive scans of the Ce 3d region performed after the XPS survey scan, we found it to be 12.9 %. This difference can be attributed to X-ray induced reduction of Ce^{4+}. However, since the XPS experiment is performed using the exact same method for all samples, this still allows for qualitatively comparing all samples, while not providing absolute Ce^{3+} concentrations.

Table S2: XPS fitting parameters CeO_2

Peak	u□□□	u□□	u(1)	u(2)	v□□□	v□□	v(1)	v(2)
Binding Energy (eV)	916.74	907.03	902.14	900.64	898.20	888.53	883.73	882.23
FWHM (eV)	2.26	3.50	2.65	1.77	2.26	4.50	2.65	1.77

Peak	u□	u(0)	v□	v0
Binding Energy (eV)	904.00	898.95	885.50	880.45
FWHM (eV)	2.40	1.80	2.40	1.80

Table S3: XPS fitting parameters CeO_2-Ar

Peak	u□□□	u□□	u(1)	u(2)	v□□□	v□□	v(1)	v(2)
Binding Energy (eV)	916.70	907.05	902.21	900.71	898.24	888.55	883.73	882.23
FWHM (eV)	2.09	3.50	2.41	1.61	2.09	4.25	2.42	1.61

Peak	u□	u(0)	v□	v0
Binding Energy (eV)	904.24	898.96	885.74	880.46
FWHM (eV)	2.20	1.80	2.20	1.80

Table S4: XPS fitting parameters CeO_2-PR

Peak	u□□□	u□□	u(1)	u(2)	v□□□	v□□	v(1)	v(2)
Binding Energy (eV)	916.62	907.11	902.16	900.66	898.17	888.61	883.68	882.18
FWHM (eV)	2.11	3.5	2.41	1.60	2.11	4.12	2.41	1.60

Peak	u□	u(0)	v□	v0
Binding Energy (eV)	904.19	898.95	885.69	880.45
FWHM (eV)	2.32	1.80	2.32	1.80

Table S5: XPS fitting parameters CeO_2-TR

Peak	u	u	u(1)	u(2)	v	v	v(1)	v(2)
Binding Energy (eV)	916.70	907.17	902.29	900.79	898.30	888.69	883.71	882.21
FWHM (eV)	2.37	4.64	2.29	1.53	2.37	4.46	2.29	1.53

Peak	u	u(0)	v	v0
Binding Energy (eV)	904.04	898.95	885.54	880.45
FWHM (eV)	2.39	2.03	2.39	2.03

Table S6: XPS fitting parameters 3wt% Cu/CeO_2

Peak	u	u	u(1)	u(2)	v	v	v(1)	v(2)
Binding Energy (eV)	916.64	907.8	902.13	900.62	898.20	888.78	883.70	882.20
FWHM (eV)	2.41	4.02	2.86	1.90	2.41	4.35	2.86	1.90

Peak	u	u(0)	v	v0
Binding Energy (eV)	903.79	898.95	885.29	880.45
FWHM (eV)	2.40	1.95	2.40	1.95

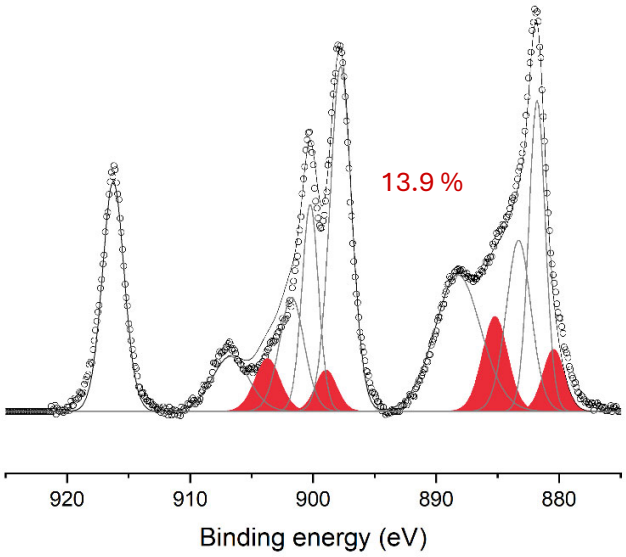

Figure S14: XPS of Ce 3d for the spent CeO_2 sample without exposure to air

Table S7: XPS fitting parameters spent CeO_2

Peak	u	u	u(1)	u(2)	v	v	v(1)	v(2)
Binding Energy (eV)	916.25	906.73	901.74	900.24	897.76	888.23	883.30	881.80
FWHM (eV)	2.08	3.50	2.37	1.58	2.08	4.41	2.37	1.58

Peak	u	u(0)	v	v0
Binding Energy (eV)	903.72	898.95	885.22	880.45
FWHM (eV)	2.40	2.04	2.40	2.04

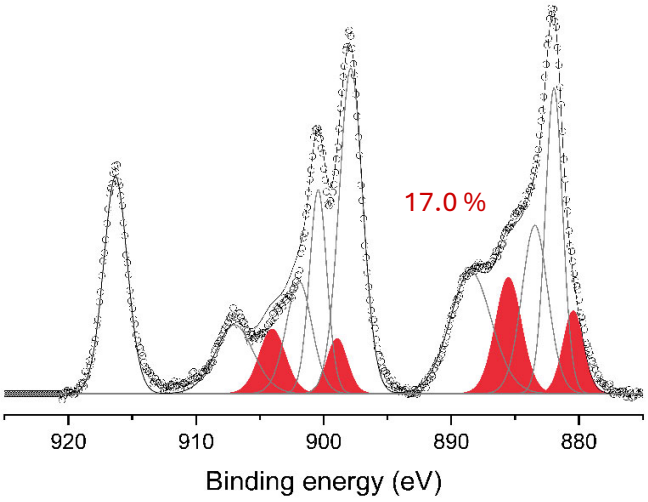

Figure S15: XPS of Ce 3d for the spent CeO_2-Ar sample without exposure to air

Table S8: XPS fitting parameters spent CeO_2-Ar

Peak	u	u	u(1)	u(2)	v	v	v(1)	v(2)
Binding Energy (eV)	916.30	906.98	901.93	900.43	897.87	888.48	883.46	881.96
FWHM (eV)	2.18	3.50	2.40	1.60	2.18	3.83	2.40	1.60

Peak	u	u(0)	v	v0
Binding Energy (eV)	904.03	898.95	885.53	880.45
FWHM (eV)	2.40	1.87	2.40	1.87

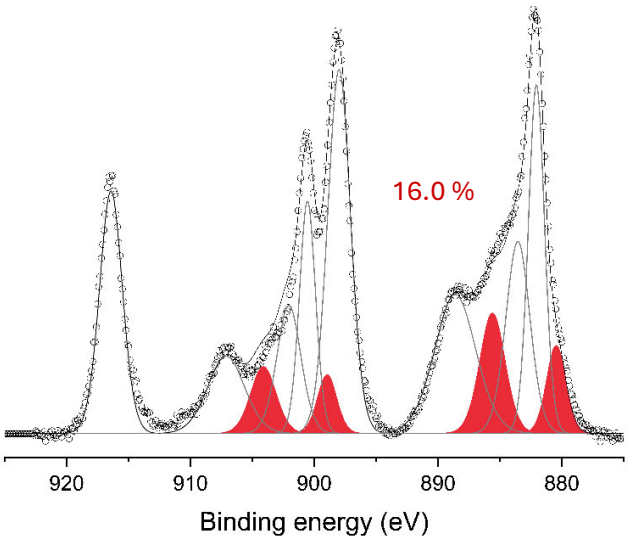

Figure S16: XPS of Ce 3d for the spent CeO_2-PR sample without exposure to air

Table S9: XPS fitting parameters spent CeO_2-PR

Peak	u'''	u''	u(1)	u(2)	v'''	v''	v(1)	v(2)
Binding Energy (eV)	916.40	907.10	902.04	900.54	897.98	888.60	883.54	882.04
FWHM (eV)	2.16	3.50	2.29	1.53	2.16	3.92	2.89	1.53

Peak	u'	u(0)	v'	v0
Binding Energy (eV)	904.10	898.95	885.60	880.45
FWHM (eV)	2.39	1.82	2.39	1.82

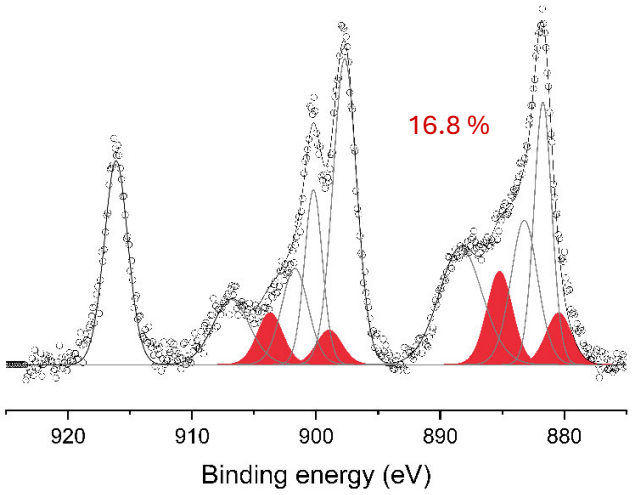

Figure S17: XPS of Ce 3d for the spent CeO_2-TR sample without exposure to air

Table S10: XPS fitting parameters spent CeO_2-TR

Peak	u	u	u(1)	u(2)	v	v	v(1)	v(2)
Binding Energy (eV)	916.12	906.85	901.71	900.21	897.69	888.34	883.23	881.73
FWHM (eV)	2.24	3.50	2.54	1.69	2.24	4.11	2.54	1.69

Peak	u	u(0)	v	v0
Binding Energy (eV)	903.72	898.95	885.22	880.45
FWHM (eV)	2.40	2.40	2.40	2.40

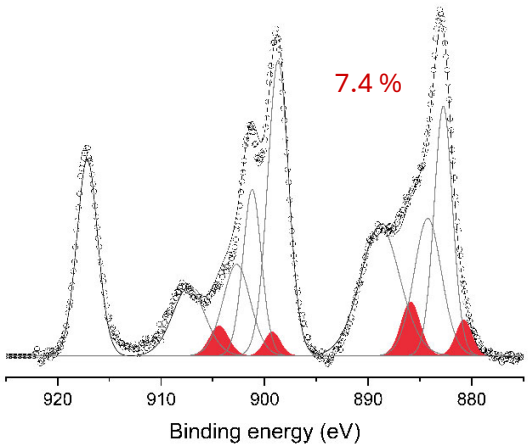

Figure S18: XPS of Ce 3d for the spent 3wt% Cu/CeO_2 sample without exposure to air

Table S11: XPS fitting parameters spent 3wt% Cu/CeO_2

Peak	u	u	u(1)	u(2)	v	v	v(1)	v(2)
Binding Energy (eV)	917.13	907.34	902.71	901.21	898.69	888.84	884.24	882.74
FWHM (eV)	2.38	3.68	3.13	2.09	2.38	4.50	3.13	2.09

Peak	u	u(0)	v	v0
Binding Energy (eV)	904.40	899.25	885.90	880.75
FWHM (eV)	2.16	1.80	2.16	1.80

S3. Discharge characterization

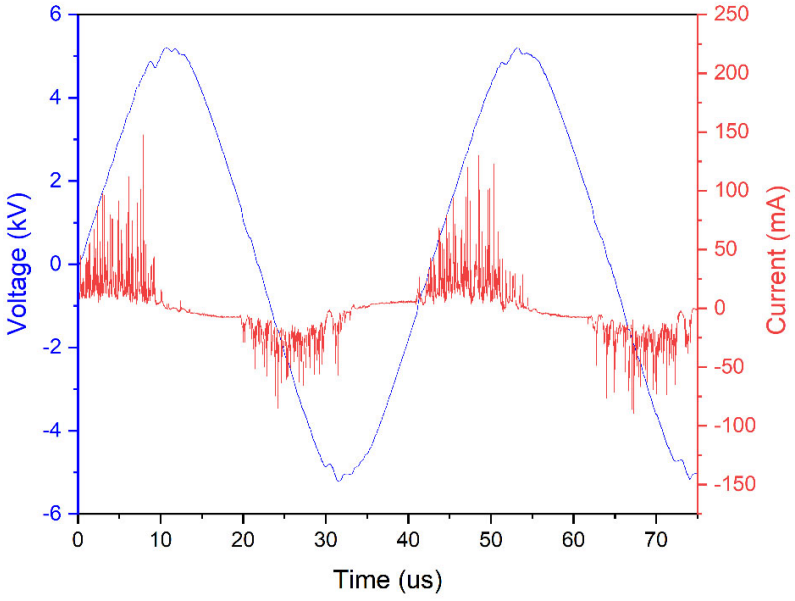

Figure S15: Representative I-V curve for the CeO_2 sample

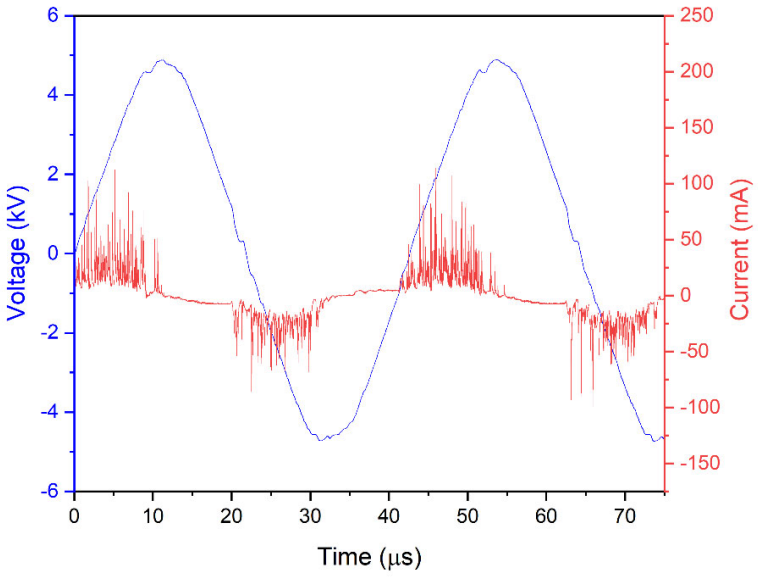

Figure S16: Representative I-V curve for the CeO_2-Ar sample

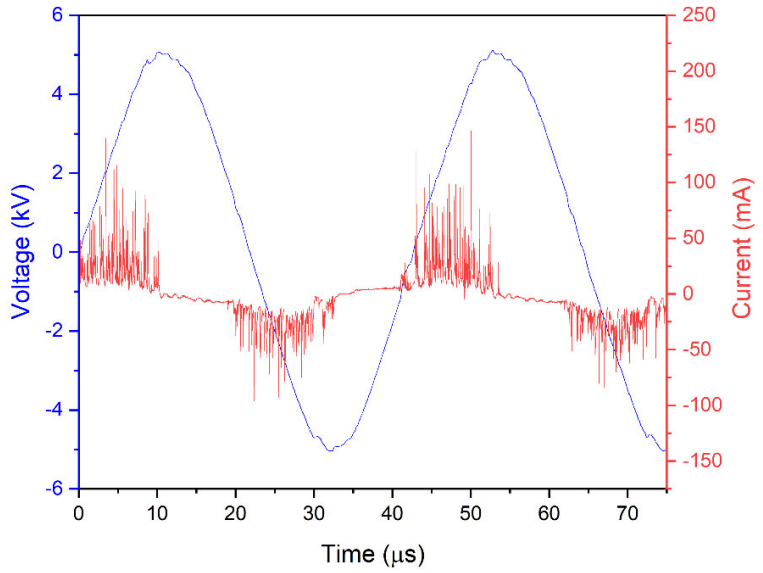

Figure S17: Representative I-V curve for the CeO_2-PR sample

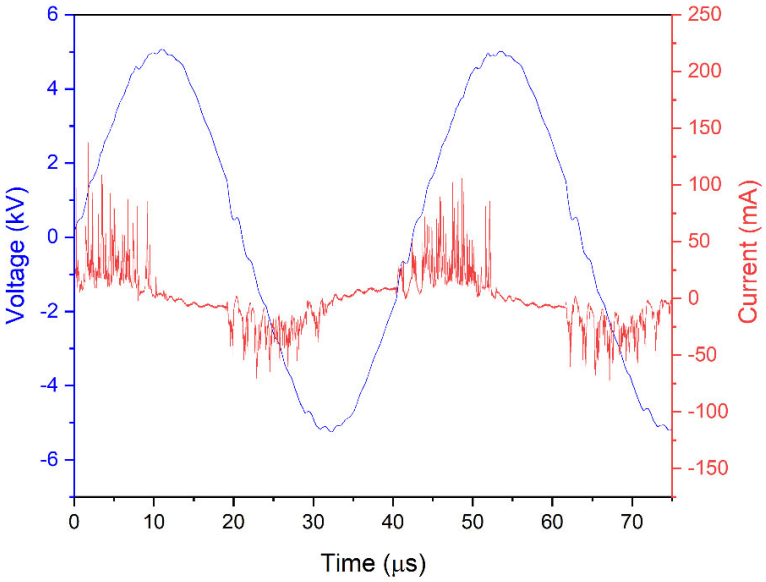

Figure S18: Representative I-V curve for the CeO_2-TR sample

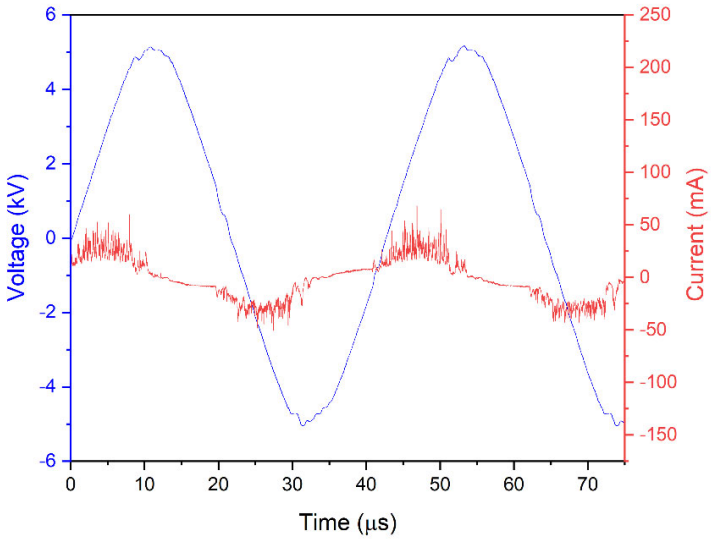

Figure S19: Representative I-V curve for the 3wt% Cu/CeO_2 sample

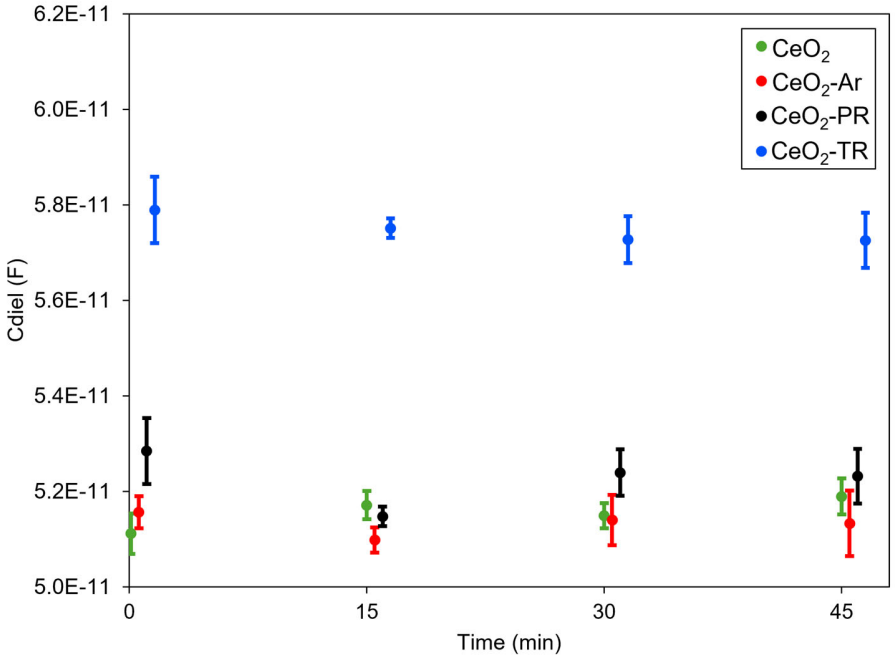

Figure S20: C_{diel} extracted from the Lissajous figures recorded during the experiments with the four different samples (see legend). Note that all measurements are taken at the same time points (0, 15, 30 and 45 min) but are slightly shifted in the graph to improve legibility

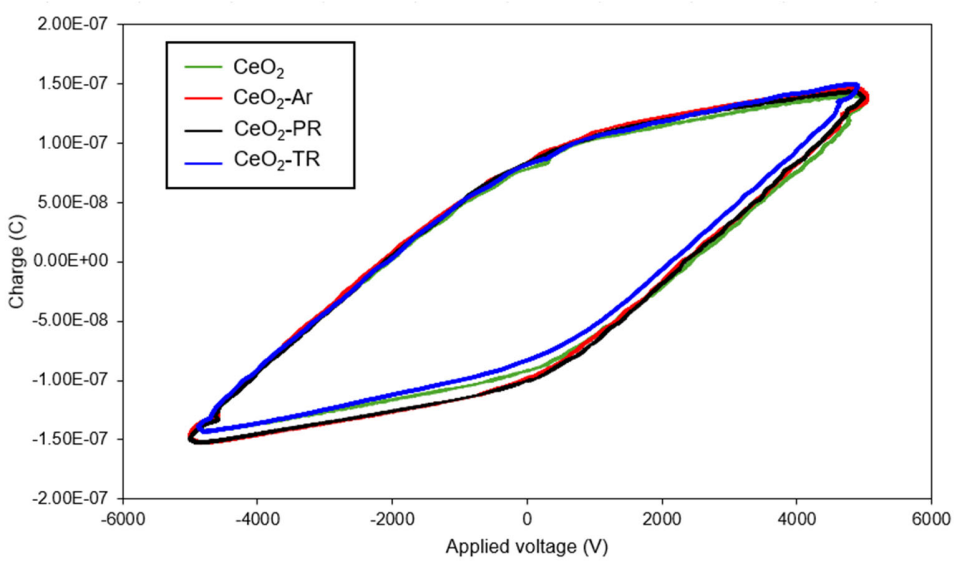

Figure S21: Representative Lissajous figures for CeO_2, CeO_2-Ar, CeO_2-PR and CeO_2-TR

S4. DFT calculations

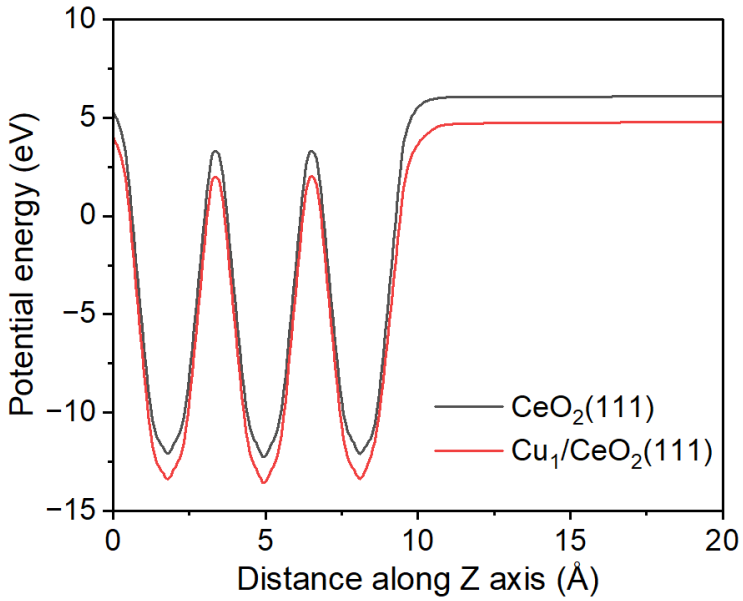

Figure S20: Planar-averaged electrostatic potential along the surface normal (Z direction) for $CeO_2(111)$ and $Cu_1/CeO_2(111)$. The Fermi level is set to 0 eV.

Reference

1. Peeters, F. J. J.; van de Sanden, M. C. M., The influence of partial surface discharging on the electrical characterization of DBDs. *Plasma Sources Science and Technology* **2014,** *24* (1).